The Low Temperature Synthesis of Very Small and Non-Crystalline Iron-Based Nanoparticles: Application in Alkene Hydrosilylation

T. Galeandro-Diamant, V. Dardun, M. Sougrati, L. Stievano, K. Lomachenko, L. Veyre, Valérie Meille, chloe Thieuleux

The low temperature synthesis of very small and non-crystalline iron-based nanoparticles: application in alkene hydrosilylation

Thomas Galeandro-Diamant,[a] Vincent Dardun,[a] Moulay Tahar Sougrati,[b] Lorenzo Stievano,[b] Kirill A. Lomachenko,[c] Laurent Veyre,[a] Valérie Meille,*[a]# and Chloé Thieuleux*[a]

[a] Université de Lyon, Institut de Chimie de Lyon, Laboratory of Catalysis, Polymerization, Processes and Materials, CP2M UMR 5128 CNRS-UCB Lyon 1-CPE Lyon, CPE Lyon 43 Bd du 11 Novembre 1918, 69616 Villeurbanne, France.
E-mail: chloe.thieuleux@univ-lyon1.fr
[b] Institut Charles Gerhardt Montpellier (ICGM), Univ. Montpellier, CNRS, ENSCM, 1919, route de Mende, 34293 Montpellier cdx 5, France
[c] European Synchrotron Radiation Facility, 71 avenue des Martyrs CS 40220 38043 Grenoble Cedex 9, France
[#] Present address: Univ Lyon, Université Claude Bernard Lyon 1, CNRS, IRCELYON, F-69626, Villeurbanne, France.
valerie.meille@ircelyon.univ-lyon1.frTitle(s), Initial(s), Surname(s) of Author(s) including Corresponding Author(s)

Supporting information for this article is given via a link at the end of the document.

Abstract: This work describes the synthesis of very small non-crystalline and non-metallic iron-based nanoparticles in solution from easily accessible commercial products in mild conditions. These colloidal suspensions were further used to generate well-defined solids containing metallic iron or iron oxide NPs. While classical magnetic and crystalline Fe nanoparticles are inactive in alkene hydrosilylation, such original NPs were active in 1-octene hydrosilylation with 1,1,1,2,3,3,3-heptamethyltrisiloxane (MD'M) showing that the non-crystallinity and the organometallic character of the starting Fe NPs are an asset to generate a specific catalytic activity.

Introduction

Many reactions are catalyzed by metallic nanoparticles (NPs), providing a performance that depends on their shape, size and composition.[1-4]
Experimental protocols are thus more and more oriented toward the synthesis of tailored NPs with precisely controlled properties.[5,9] The synthesized NPs show an expected crystallinity and their activity can be correlated with the number of facets, edges or corners.[6] In our approach, the objective is not to obtain crystalline NPs, and we were curious to specifically evaluate the performance of non-crystalline systems. In this context, we recently published the development of Ni silicides and cobalt nano-aggregates which demonstrated the interest of amorphous phases in CO_2 reforming of methane[10] and alkene hydrosilylation.[11,12] In the present work, iron NPs were targeted. Indeed, the synthesis and use of iron nanoparticles in catalysis has led to an increased interest in recent years with the development of protocols leading to crystalline iron NPs with different shapes and sizes.[13–15] In this context, we report here the preparation of very small zero-valent iron nanoparticles (1-2 nm) following a very simple protocol avoiding the use of surfactants or classical stabilizing agents (such as phosphine or amine) as well as that of high temperature boiling solvent (such as oleic acid or polyols) classically reported in the literature. Such iron NPs resulted very different from those described in the literature: they are remarkably small, non-metallic and non-crystalline as described hereafter, where their properties are analyzed in detail and related to their physico-chemical and structural features.

Results and Discussion

Iron colloids were synthesized by reaction of an iron carbonyl complex, $Fe_3(CO)_{12}$, with *n*-octylsilane in toluene using atomic ratio Fe : Si = 1 : 1 and temperatures from 80 °C to 140 °C under 3 bars of H_2 (Scheme 1).

$$Fe_3(CO)_{12} + \textit{n}\text{-octylsilane} \xrightarrow{\text{Toluene, 3 bars } H_2\text{, 80-140 °C}} \text{Fe colloids}$$

Scheme 1. Synthesis of Fe NPs.

Three different colloidal suspensions of Fe NPs were obtained as listed in Table 1. The NPs are all very small in size (1.6 to 2.9 nm), with a very narrow size distribution as demonstrated by the histograms extracted from HAADF-STEM images presented in Figure 1 (histograms can be found in ESI). Note that an increase of the size from 1.6 nm to 2.9 nm is observed when the reaction temperature is increased.

Table 1. Different colloidal solutions prepared and NPs' size

Conditions	Colloid **1**	Colloid **2**	Colloid **3**
T/°C	80	120	140
Fe:Si ratio	1:1	1:1	1:1
NPs' size (nm)	1.6 ± 0.3	2.6 ± 0.7	2.9 ± 0.5

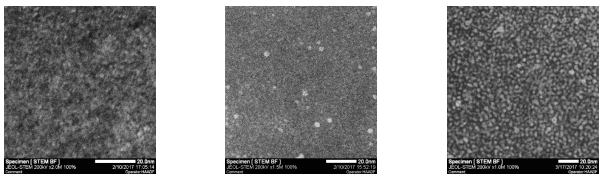

Colloid**1** Colloid**2** Colloid**3**

Figure 1. HAADF-STEM images of Fe nanoparticles in suspension.

UV-visible spectroscopy was used to monitor the decomposition of the $Fe_3(CO)_{12}$ precursor which leads to the formation of the NPs. The spectra of the colloidal suspensions do not exhibit the characteristic signal of the Fe precursor at 600 nm (Figure 2). This result clearly indicates the complete decomposition of the starting precursor.

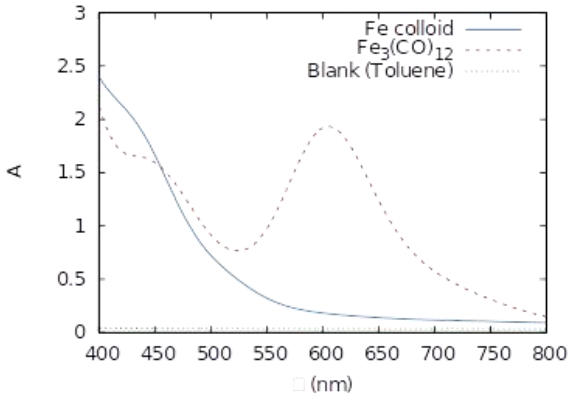

Figure 2. UV spectra of Colloid **1** and $Fe_3(CO)_{12}$

IR spectroscopy was applied to further characterize the as-obtained Fe colloids. Their spectra (Figure 3), compared to that of $Fe_3(CO)_{12}$, highlight the disappearance of the terminal and bridging carbonyl bands of the iron carbonyl precursor around 2100 cm^{-1} (intense and sharp signal corresponding to terminal CO[16]) and 1850 cm^{-1} (broad and very weak signal corresponding to bridged CO) and the appearance of several new terminal CO bands (broad signals) from 1860 to 2100 cm^{-1} for Colloid **1** and **2**. This broad signal was very weak in the case of Colloid **3**, suggesting a very small amount of Fe surface sites able to coordinate CO in comparison with Colloids **1** and **2**.

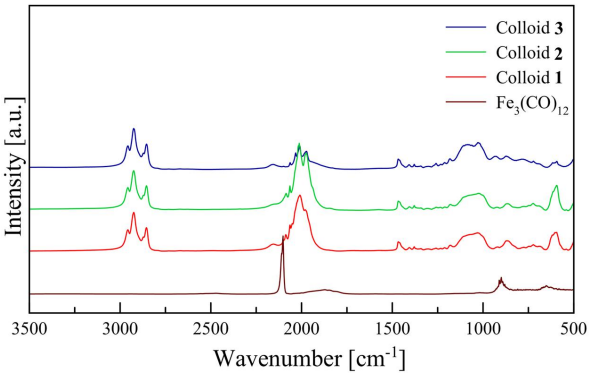

Figure 3. IR spectra of Colloid **1**, Colloid **2**, Colloid **3** and $Fe_3(CO)_{12}$. The colloid spectra were obtained after mixing in dry KBr under inert atmosphere and toluene evaporation under vacuum and the signal intensity of the different spectra was normalized with the ν(C-H) band at 2926 cm^{-1} (considering that the Fe:Si ratio is the same for all the materials and thus the C-H fragments also).

For a deeper characterization of the colloids, low temperature (5 K) ^{57}Fe Mössbauer spectroscopy was used and, to facilitate such experiments, the Fe NPs were deposited on silica by incipient wetness impregnation under rigorous inert atmosphere and dried under vacuum prior to their analysis in sealed cells to avoid Fe oxidation (See ESI for details). The solid sample from impregnation of Colloid **1** is quoted RawSolid in the last part of this manuscript.

The Mössbauer spectrum of Colloid **1** (RawSolid) at 5 K exhibits a dominant broad signal corresponding to 98.6 % of the total absorption area. It was fitted with three different contributions with isomer shifts (IS) centered around 0 mm/s and quadrupole splittings (QS) of 1.49, 0.52, 1.00 mm/s, respectively (Figure 4 & Table 2). Even though these values are not identical to known carbonyl compounds such as $Fe_3(CO)_{12}$ or $Fe_2(CO)_9$, they fall in the typical range of iron carbonyls.[17] In particular, the spectrum is different from that of the $Fe_3(CO)_{12}$ precursor, which contains two distinct contributions attributed to two different iron sites in the cluster; a very narrow quadrupole doublet with almost no quadrupole splitting representing the iron center bound only to terminal carbonyls, and a relatively large doublet (QS = 1.15 mm/s) which is attributed to two iron atoms bound to terminal and bridging carbonyls.[18]
The hyperfine parameters of the spectrum of Colloid **1** (Table 2) suggest that this colloid consists of multinuclear iron carbonyl species containing a neutral iron metal core and terminal as well as bridging carbonyls.[19] The broadness of this spectral signal (fitted with three contributions) highlights the existence of multiple slightly different iron sites, possibly sitting in the core or at the surface of the particles, and/or representing different carbonyl coordination environments. Indeed, our group used ^{119}Sn Mossbauer spectroscopy to show that surface tin atoms of $PtSn_3/SiO_2$ catalysts containing very small $PtSn_3$ nanoparticles gave a signal with a large quadrupole splitting, distinct from the signal of Sn atoms in the bulk $PtSn_3$.[20] This large quadrupole splitting was explained by the "anisotropy of the electron cloud" around the ^{119}Sn nuclei located at the surface of the NPs. Given that our Fe NPs are very small, the same phenomenon may be present here and the surface Fe atoms could be responsible of some of the iron sites involved in the large spectral distribution. The additional minor spectral contribution (1.4 % of the total absorption area) observed in the Colloid **1** spectrum, can be attributed to a high-spin Fe(II) impurity, probably coming from a very slight oxidation of the colloid sample. Colloid **2** exhibits a Mössbauer spectrum similar to that of Colloid **1,** showing a broad dominant contribution corresponding to 86.5 % of the total absorption area vs 98.6 % for Colloid **1**. This major signal was best fitted with three distinct contributions as for Colloid **1** which isomer shifts and quadrupole splittings (see Table 2) fall in the typical range of iron carbonyls. The comparison of spectra recorded at 5 K and 300 K shows a weak Lamb-Mössbauer factor which decreases with the temperature. This reveals weak bonds, likely of organometallic type. The Debye temperature was also estimated from 112 K to 129 K depending on the fit chosen (see ESI), a very low value if compared to classical Fe metallic NPs (usually above 300 K), reinforcing the putative non-crystalline and organometallic nature of the NPs. The additional minor spectral contribution representing to 14.5 % of the total absorption area is attributed to a high-spin Fe(II) species, suggesting that an increase of the colloid preparation temperature leads to a decrease of the iron carbonyls content and the emergence of oxidized species namely high-spin Fe(II) species. In the case of Colloid **3**, the Mössbauer spectrum, also shown in Figure 4, was found substantially different and consists of several contributions representing different iron states. A large distribution of hyperfine fields, centered at 0.44 mm/s and counting for about 73 % of the total absorption area, represents ill-defined Fe(III) oxide-like species which do not undergo

complete magnetic ordering at 5 K. This major component is accompanied by two additional ones, the first one is very similar to the main component in Colloid **1** and Colloid **2** and was thus attributed to iron carbonyl species and the second one to traces of Fe(II). From these results, one can conclude that an increase of the temperature used for the colloids preparation leads to a drastic modification of the nanoparticles composition with a decrease of the iron carbonyls content which Mössbauer contribution is now representing only 20.7 % of the total absorption area along with the emergence of oxidized Fe species of which a major amount of Fe(III) accounting for 73 % of the total absorption area and a minor amount of Fe(II) accounting for 6.3 % of the total absorption area.

Table 2. ^{57}Fe hyperfine parameters at 5 K for the measured colloids

Spectrum	Comp.	IS (mm/s)	QS (mm/s)	LW (mm/s)	B_{HF} (Tesla)	Abs (%)
Colloid **1**	$Fe_x(CO)_y$ (1)	-0.02	1.49	0.41	-	20.6
	$Fe_x(CO)_y$ (2)	-0.05	1.00	0.41	-	35.4
	$Fe_x(CO)_y$ (3)	-0.04	0.52	0.48	-	42.5
	Fe^{2+}	0.92	2.75	0.2	-	1.4
Colloid **2**	$Fe_x(CO)_y$ (1)	-0.03	1.33	0.39	-	25.5
	$Fe_x(CO)_y$ (2)	-0.05	0.88	0.39	-	29.4
	$Fe_x(CO)_y$ (3)	-0.08	0.50	0.45	-	30.6
	Fe^{2+}	1.38	1.74	1.2	-	14.5
Colloid **3**	$Fe_x(CO)_y$	-0.02	0.86	0.80	-	20.7
	Fe^{2+}	1.24	1.27	0.80	-	6.3
	Fe^{3+}	0.44	-	0.80	38.3	73.0

To further get insight into the chemical nature of the colloids, X-ray absorption measurements were also conducted at BM23 beamline[21] of the ESRF using $Fe_3(CO)_{12}$ and Fe(foil) as references.

Overall, the XANES and EXAFS spectra of Colloid **1** and Colloid **2** appear very similar to that of $Fe_3(CO)_{12}$ (Figures 5 and 6) which is in line with the non-crystalline nature of the Fe NPs for such colloids.

At the reverse, the spectrum obtained for Colloid **3** (Figure 5 and 7) completely differs from that of the iron carbonyl precursor and is also strongly different from that of the Fe foil. The fitting of the EXAFS spectra of Colloids **1** and **2** (Table 3 and ESI) allowed a rough estimate of the Fe neighbouring atoms and the results show the presence of carbon and oxygen atoms suggesting the presence of CO ligands and the presence of neighbouring Fe atoms (Fe-Fe bonds).

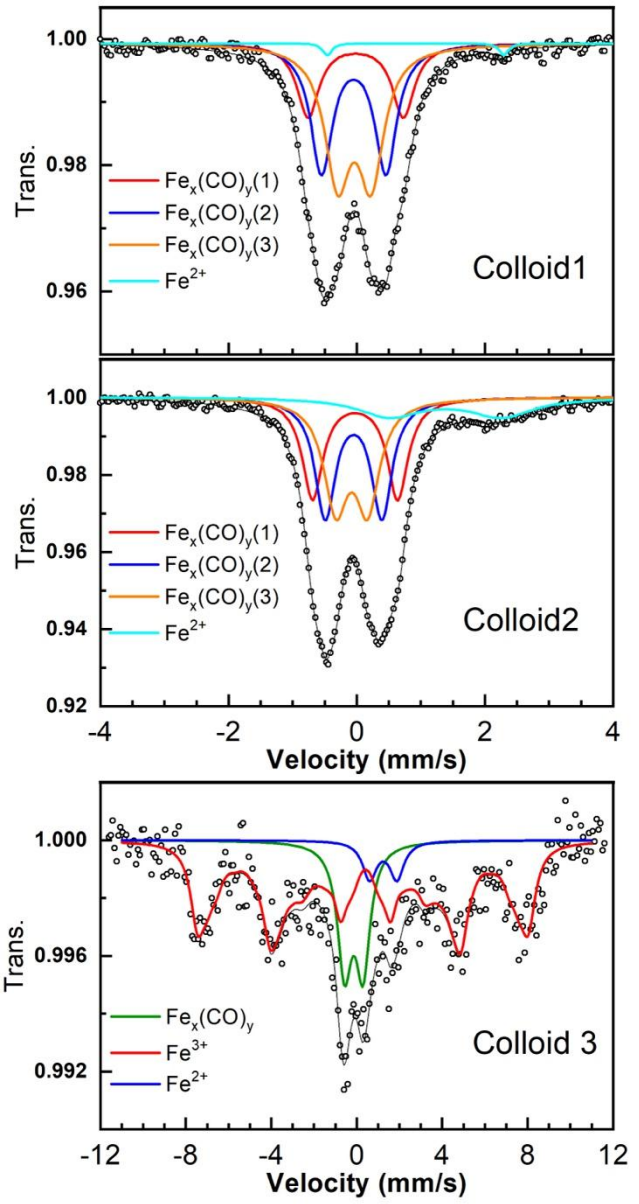

Figure 4. ^{57}Fe Mössbauer spectra of Colloid **1** (top), Colloid **2** (middle) and Colloid **3** (bottom) measured at 5 K.

These results thus strongly confirm the non-crystalline nature of the Fe NPs and their rather organometallic character (as already suggested by Mössbauer spectroscopy). These Fe NPs may be considered as nano-aggregates of iron and carbonyl ligands $Fe_x(CO)_y$ possibly stabilized by surface alkylsilane fragments. Note that the absence of Fe-Si contribution can be explained by the fact that the silicon atoms are only localized at the nanoparticles surface and that the NPs are not composed of bulk Fe-silicide phase.

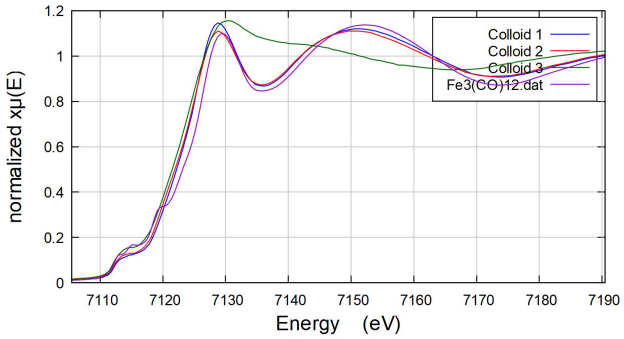

Figure 5. The *q*-space XANES spectra of Colloids **1**, **2** and **3**, $Fe_3(CO)_{12}$.

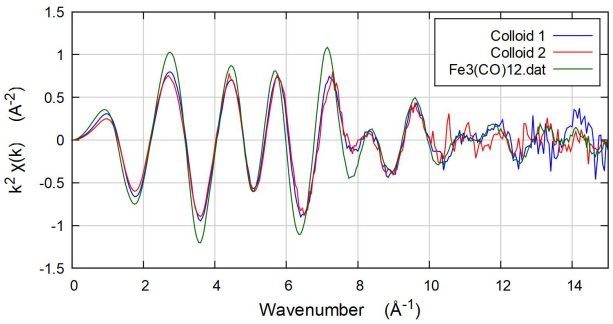

Figure 6. The *k*-space EXAFS spectra of Colloid **1**, Colloid **2** and $Fe_3(CO)_{12}$.

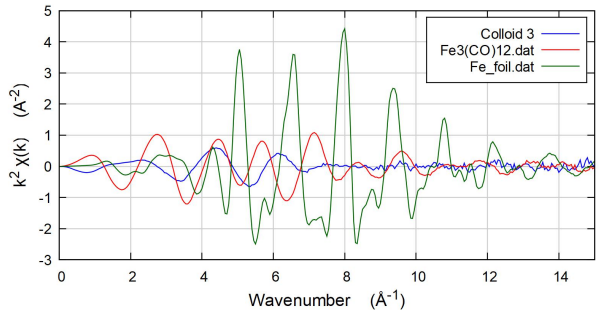

Figure 7. The k-space spectra of Colloid **3**, $Fe_3(CO)_{12}$ and Fe foil.

The EXAFS spectrum of Colloid **3**, on the contrary, could not be fitted without introducing a dominant contribution of Fe-O nearest neighbors, which represent ill-defined iron oxide species that count for about ¾ of the total spectrum. This result, in agreement with Mössbauer spectroscopy, shows that this sample mainly consists of oxidized Fe(III) species.

Table 3. Fitting parameters obtained from simulation of the EXAFS data of Colloids **1**, **2, 3** and $Fe_3(CO)_{12}$

Sample	Shell	N	S_0^2	σ^2	R (th.)	R (exp.)
colloid **1**	Fe-C(1)	3	1	0.0051(4)	1.8525	1.802(4)
	Fe-C(2)	2.5	1	0.0051(4)	2.2123	2.109(7)
	Fe-Fe	2	1	0.011(1)	2.6328	2.623(9)
	Fe-O	7.667	1	0.0037(4)	3.0225	3.021(7)
colloid **2**	Fe-C(1)	3	1	0.0060(8)	1.8525	1.790(9)
	Fe-C(2)	2.5	1	0.0060(8)	2.2123	2.10(2)
	Fe-Fe	2	1	0.012(2)	2.6328	2.59(2)
	Fe-O	7.667	1	0.0035(7)	3.0225	3.01(1)
colloid **3**	Fe-C	5	0.27(8)	0.02(8)	1.8525	1.83(8)
	Fe-Fe	2	0.27(8)	0.008(3)	2.8328	2.54(3)
	Fe-O	6	0.27(8)	0.004(3)	3.0225	3.03(4)
	Fe-O (ox)	6	0.73(8)	0.019(3)	2.0500	2.02(5)
$Fe_3(CO)_{12}$	Fe-C(1)	3.333	1	0.0044(4)	1.8525	1.821(5)
	Fe-C(2)	1.333	1	0.0044(4)	2.2123	2.14(2)
	Fe-Fe	2	1	0.0070(6)	2.6328	2.643(8)
	Fe-O	7.667	1	0.0022(5)	3.0225	3.039(8)

From Colloid **1**, several heterogeneous catalysts containing metallic iron and iron oxide NPs were prepared as described in Figure 8. The best procedure to secure the dispersion and the small size of the Fe NPs consisted into incipient wetness impregnation of the colloidal suspension onto silica under argon followed by appropriate oxidative or reductive thermal treatments. The initial green-brown solid, called RawSolid, resulted from the colloid impregnation onto silica under argon and drying under vacuum. A second deep brown solid, called OxidizedRT, was obtained by dry air oxidation of the RawSolid at room temperature. A third orange solid, named Oxidized500, was obtained by calcination at 500 °C under dry air flow of the OxidizedRT solid. A fourth grey solid, Reduced500, was obtained by reduction of the Oxidized500 solid under H_2 flow at 500 °C. Finally, a fifth deep grey solid, quoted Reduced500Direct, was obtained by treatment of the RawSolid under H_2 at 500 °C (without exposure to air prior to the treatment).

Characterization of the Reduced500 solid by TEM (Figure 9) revealed that the particles were small and well-dispersed with a mean diameter of ca. 2.5 nm.

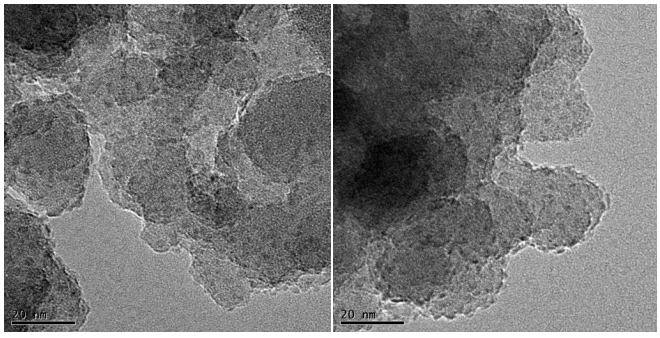

Figure 9. TEM micrographs of Reduced500 solid.

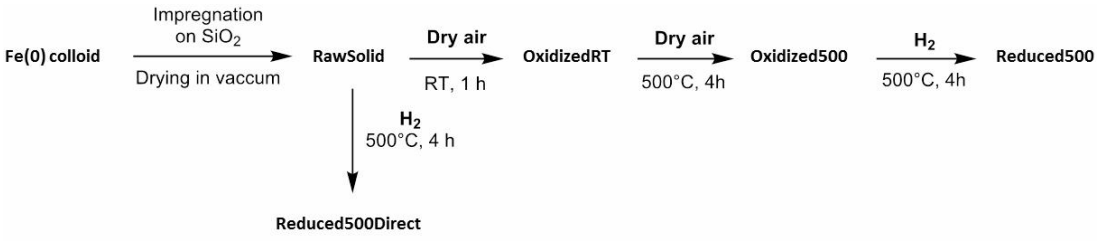

Figure 8. Preparation route for the heterogeneous catalysts

The Reduced500Direct solid was also characterized by TEM (Figure 10), showing Fe NPs with a diameter of 2.0-2.5 nm. Note that the intermediate solids (OxidizedRT and Oxidized500) also exhibited small Fe NPs. However, the contrast was too low to reliably establish a size distribution histogram.

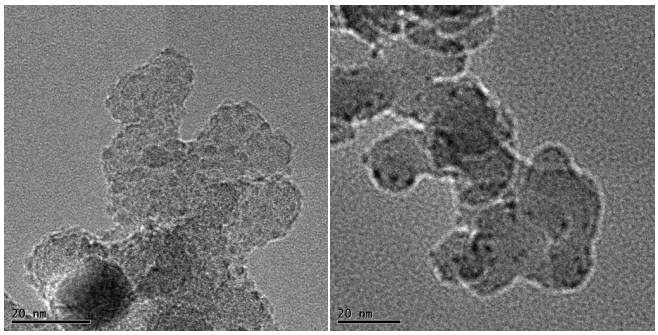

Figure 10. TEM micrographs of Reduced500Direct solid.

Overall, there is no significant difference in the size of Fe NPs in the different observed solids, which indicates the absence of sintering during thermal treatments.

^{57}Fe Mössbauer spectroscopy was performed at room temperature on the Fe-containing solids after thermal treatments (Figure 11 and Table 4).

The OxidizedRT solid featured two signals attributed to ill-defined Fe(III) species with different quadrupole splittings, indicating the presence of higher distortion in the coordination of the component with the largest quadrupole splitting. Despite these slight differences, one can conclude that, even at room temperature, all Fe atoms were directly oxidized to Fe(III). The Oxidized500 solid was found very similar to the OxidizedRT solid, except that the Fe(a) component with a high quadrupole splitting is more intense. Moreover, a slight increase of the average quadrupole splittings for the two components (Fe(a) and Fe(b)) indicates an increase in the distortion of the two iron sites. These two components might, for example, correspond to atoms at the surface of the NPs (Fe(a)), more coordinatively unsaturated than in OxidizedRT solid since the stabilizing silane ligands originally present at the surface were removed by the calcination at 500 °C and not by exposure to air at RT.

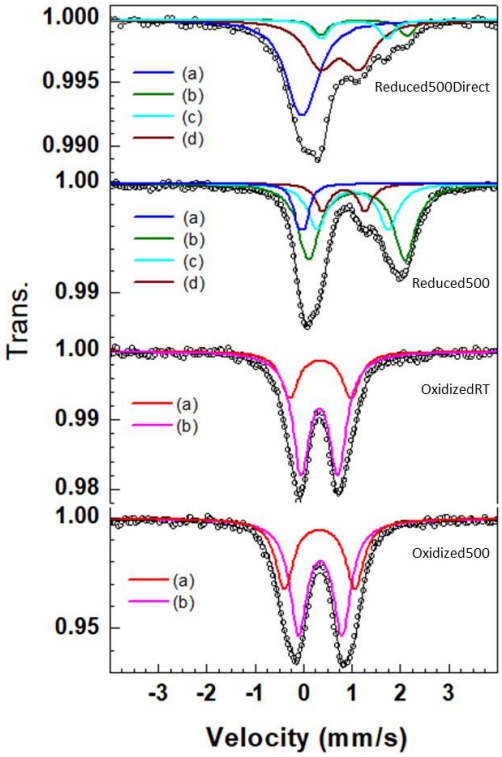

Figure 11. ^{57}Fe Mossbauer spectra (black) at RT of the four heterogeneous catalysts after thermal treatments with possible contributions in colored lines.

The Reduced500 solid featured one Fe(a) signal, attributed to metallic superparamagnetic Fe(0) species accounting for 10 % of the total absorption area. The Fe (b) and Fe(c) signals, representing 80 % of the total absorption area, have similar isomer shifts that could correspond to high spin Fe(II) centers showing that the reductive treatment did not allow the complete reduction of the sample that was previously oxidized under dry air flow at 500 °C. The Fe(d) signal is more difficult to attribute to a specific iron species. Indeed, superparamagnetic iron nanoparticles usually exhibit at room temperature a spectral feature representing iron atoms at the surface of the particles, with a broad quadrupole splitting doublet and hyperfine parameters not very different from those of high spin Fe(III).[22] For sample Reduced500, the value of the isomer shift for this component is higher than expected for a pure surface iron component, but still substantially lower than that of divalent iron. Such a component could thus be attributed to iron surface species in a non-classical environment as Fe silicides for instance, but also to iron species in an oxidation state between Fe(II) and Fe(III). Unfortunately, the spectrum at low temperature of this sample could not be measured, which leaves an uncertainty in the interpretation of the exact nature of this

component. The Reduced500Direct solid exhibits the same spectral component of Reduced500, but with a Fe(a) contribution corresponding to metallic superparamagnetic Fe(0) centers accounting for about half of the Fe atoms. Similarly, the ill-defined Fe(d) component corresponds to 38 % of the total absorption area; the simultaneous important increase of both Fe(a) and Fe(d) in such a more reduced sample suggests that the two components are connected, and that Fe(d) may indeed represent surface iron species in a non-classical environment. The two other very minor signal (Fe(b) and Fe(c)) corresponding to Fe(II) species could be related to the partial oxidation of the sample during the preparation and/or the analysis.

Table 4. ^{57}Fe Mossbauer data for the solid samples

Spectrum	Comp.	IS (mm/s)	QS (mm/s)	LW (mm/s)	Abs (%)	Attribution
Reduced500Direct	(a)	-0.03	0.2	0.68	46.1	Fe^0
	(b)	1.24	1.78	0.31	6.9	Fe^{2+}
	(c)	1.04	1.36	0.33	8.2	Fe^{2+}
	(d)	0.75	0.80	0.71	38.8	$Fe_{(surf.)}$
Reduced500	(a)	-0.05	0.15	0.58	10.0	Fe^0
	(b)	1.1	1.98	0.52	51.0	Fe^{2+}
	(c)	1.02	1.47	0.47	28.5	Fe^{2+}
	(d)	0.83	0.87	0.31	10.5	$Fe_{(surf.)}$
OxidizedRT	(a)	0.35	1.27	0.43	28.0	Fe^{3+}
	(b)	0.32	0.76	0.43	72.0	Fe^{3+}
Oxidized500	(a)	0.33	1.46	0.44	38.3	Fe^{3+}
	(b)	0.34	0.90	0.44	61.7	Fe^{3+}

Overall, the deposition of colloid **1** onto silica and further appropriate thermal treatments allows the conversion of the Fe_xCO_y nano-aggregates into heterogeneous catalysts that contain small iron NPs that could be either metallic Fe NPs (Reduce500Direct), to iron (II) NPs (Reduced500) or to iron oxide Fe(III) NPs (OxidizedRT and Oxidized500).

Catalytic tests

The original features of the synthesized NPs in solution and the corresponding solids after thermal treatments prompted us to test them as catalysts for the hydrosilylation of 1-octene with a benchmark tertiary silane relevant for industry, namely 1,1,1,2,3,3,3-heptamethyltrisiloxane (MD'M) as shown in Figure 12. A first experiment was performed at 120 °C with Colloid **1** at a Fe loading of 2 mol%. The 1-octene conversion was more than 90 % after 6 h (Figure 13), with a yield in silylation products of ca. 10 %. The conversion of MD'M was low compared to that of 1-octene (20:90), due to a rapid isomerization of 1-octene.

Note that, in this area, literature examples exhibiting the use of iron colloids as catalysts for olefin hydrosilylation are scarce. In 1962, a pioneer article from Nesmeyanov *et al.* disclosed the use of an iron colloid (from decomposition of iron carbonyl at 220°C in naphthalene) as catalyst for the hydrosilylation of one single activated silane, namely methyldichlorosilane (CH_3SiCl_2H) with ethylene or propylene. Unfortunately, the catalytic performance were very disappointing and no characterization of the particles was provided.[23] Only 55 years later (i.e. in 2018), Azuma *et al.* developed DMF-stabilized iron oxide nanoparticles as active hydrosilylation catalysts[13]. However, the catalytic performances were limited to the hydrosilylation of a highly activated silane, namely phenyltrihydrogenosilane ($PhSiH_3$).

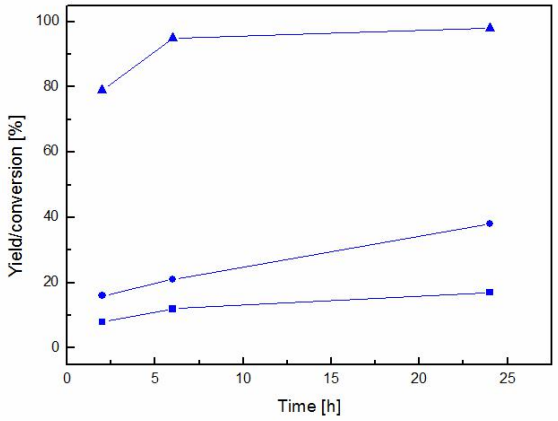

Figure 13. Transformation of 1-octene with MD'M (1:1 ratio) at 120 °C with 2 mol% Fe (Colloid **1**). The triangles correspond to 1-octene conversion, the circles correspond to MD'M conversion, and the squares correspond to the overall yield of both hydrosilylation and dehydrogenative silylation.

Another experiment was thus performed at a higher octene/SiH ratio (2:1) and at room temperature with a very low Fe loading of 0.2 mol% (Figure 14); the yield in silylation product was still limited by the total conversion of 1-octene due to isomerisation. However, the hydrosilylation/dehydrogenative silylation yield increased to 20 %, which is remarkable for Fe NPs at RT. A unusual products distribution was also observed with the linear hydrosilylation product as the major product along with different isomer-products of dehydrogenative silylation (see ESI for details). Note that no other side products were detected (no hydrogenated product of the starting olefin and no silicon oligomers). Colloid **1** and Colloid **2** exhibited very similar activities showing that the slight variation in the NP size is not playing a key role. Finally, Colloid **3**, much more similar to classical Fe NPs and which was shown to be strongly oxidized, was completely inactive. As suggested by the aforementioned results, the unexpected catalytic performance of Colloids **1** and **2** could be correlated to the non-crystallinity and the organometallic character of the NPs.

For sake of comparison, the corresponding supported NPs (RawSolid) were tested and they showed similar catalytic performance, exhibiting more than 20 % of hydrosilylation and dehydrogenative silylation yield with similar products distribution after 24 hours of reaction at room temperature. For further comparison, the four other iron phases on silica (either oxidized or reduced) showed no hydrosilylation activity. However, the Reduced500Direct sample presented a high 1-octene isomerisation activity. These results strongly suggest that neither oxidized Fe (III), Fe(II) nor metallic Fe (0) NPs were able to perform the hydrosilylation of 1-octene with MD'M and that only the colloids prepared at the lowest temperatures (Colloids **1** and **2**) could be used as catalysts for such a challenging reaction.

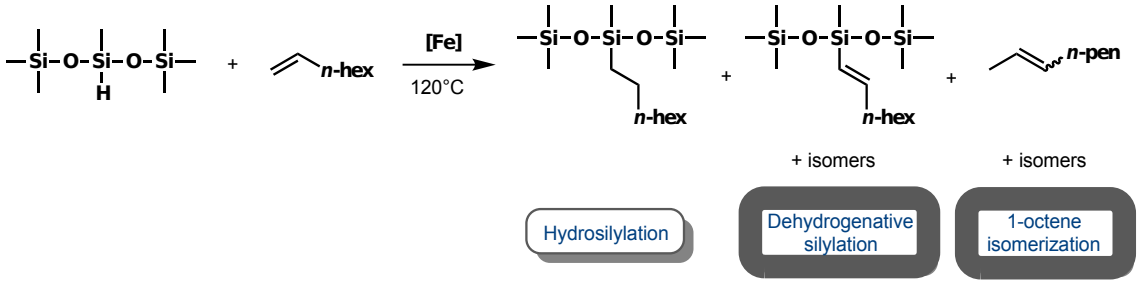

Figure 12. 1-octene hydrosilylation with MD'M

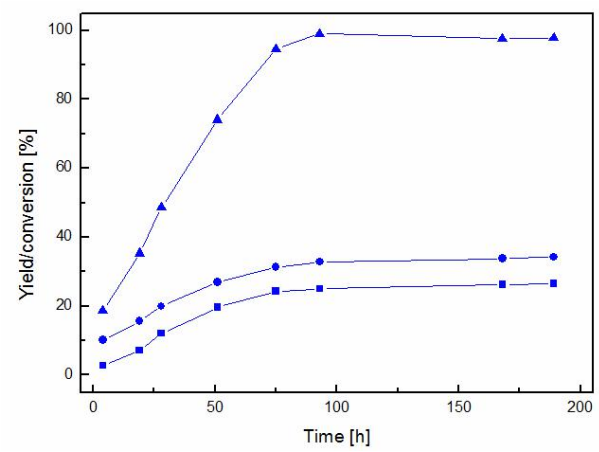

Figure 14. Transformation of 1-octene with MD'M (2:1 ratio) at RT with 0.2 mol% Fe (Colloid **1**). The triangles correspond to 1-octene conversion, the circles correspond to MD'M conversion, and the squares correspond to the overall yield of both hydrosilylation and dehydrogenative silylation.

Conclusions

This work shows that the development of experimental procedures enabling the preparation of very small non-crystalline NPs with a narrow size distribution can be of interest to generate new catalytic systems with a specific activity/behavior. This was exemplified here with the development of non-crystalline Fe NPs that were found active in hydrosilylation of 1-octene with MD'M. However, it is worth noting that such non-crystalline nanoparticles exhibited an unusual products distribution with the linear hydrosilylation product as the major product along with different isomer-products of dehydrogenative silylation. Even if the reported performance does not compete with that of state-of-the-art iron catalysts (mainly molecular complexes specifically designed for this type of reactions),[23-26] the fact that these non-crystalline nanoparticles were able to hydrosilylate octene with MD'M, when metallic and crystalline nanoparticles are inactive, opens the way to the development of a new family of materials with still unknown properties, and is therefore very interesting *per se*. This result also opens the way to the development of non-classical NPs for specific applications otherwise inaccessible with classical crystalline NPs. Finally, it was also demonstrated that such Fe NPs in solution could be further easily introduced onto silica supports yielding solids containing highly dispersed and small iron or iron oxide NPs.

Experimental Section

Catalyst preparation

A typical procedure is the following: a 500 mL Fischer-Porter reactor with a magnetic stir bar was charged with 138.5 mg of $Fe_3(CO)_{12}$ in the glovebox and 25 mL of dry toluene were added, giving a deep green solution. 156 µL of *n*-octylsilane were then added (ρ = 0.746 g/mL, Fe:Si = 1:1). The solution was heated up in a silicon oil bath to 80 °C under 3 bars static pressure of H_2. After 24 h under these conditions, the color changed to yellow-brown. The final colloidal solution was cannulated into a Schlenk flask under Ar and stored in the fridge. Its Fe loading reaches 33 µmol/mL.

Fe NPs impregnation on silica

27.2 mL of Fe colloid were concentrated under reduced pressure until reaching a volume of 1.5 mL. The solution was then added using the classical incipient wetness impregnation method.[33] It consisted of the drop-by-drop addition of the solution to 1 g of compacted fumed silica under stirring. The brown solid was further dried under vacuum (10-5 mbar) at room temperature during 1 day. It contained 5 wt% of Fe.

Catalytic tests for colloidal suspension

Catalytic tests were carried out in a Schlenk tube under Ar. In a typical procedure, 1.36 mL (5 mmol) of MD'M, 0.77 mL (5 mmol) of 1-octene and 0.5 mL of *n*-dodecane were put in a Schlenk tube containing a magnetic stirring bar. To this mixture, 3 mL of the Fe colloidal suspension were added and the reaction mixture was heated at 120 °C for 24 h. The reaction was cooled down and an aliquot was taken *via* a syringe equipped with a filter. GC analysis was performed in order to determine the catalytic performance.

Catalytic tests for silica-supported NPs

Catalytic tests were carried out in a Schlenk tube under Ar. In a typical procedure, 1.36 mL (5 mmol) of MD'M, 0.77 mL (5 mmol) of 1-octene, 0.5 mL of *n*-dodecane and 111 mg of silica-supported catalyst (0.1 mmol of Fe, 0.02 eq) were put in a Schlenk tube containing a magnetic stirring bar. The reaction mixture was heated at 120 °C for 24 h. Samples were regularly taken, filtered, exposed to air and analysed by GC.

Acknowledgements

This research was performed in the frame of French collaborative projects funded by the French National Research Agency (ANR) (grant number ANR-18-CE07-0021 (HYPERCAT) ; grant number ANR-13-CDII-0007 (HYSINANO)) and we gratefully thank the ANR and the CNRS for funding and support. There are no conflicts to declare.

Keywords: Iron • nanoparticles • hydrosilylation • catalysts • colloids

[1] Z. Wu, S. Yang, W. Wu, *Nanoscale* **2016**, *8*, 1237–1259.
[2] S. Cao, F. Tao, Y. Tang, Y. Li, J. Yu *Chem. Soc. Rev.* **2016**, *45*, 4747–4765.
[3] K. An, G. A. Somorjai ChemCatChem2012, 4, 1512–1524.
[4] X. Wang, N. Liu, R. Xu, B. Chen, C. Dai, B. Wu, G. Yu, *Appl. Surf. Sci.* **2021**, *536*, 147844.
[5] O. Margeat, F. Dumestre, C. Amiens, B. Chaudret, P. Lecante, M. Respaud, *Prog. Solid State Chem.* **2005**, *33*, 71–79.
[6] L. M. Lacroix, S. Lachaize, A. Falqui, M. Respaud, B. Chaudret, *J. Am. Chem. Soc.* **2009**, *131*, 549–557.
[7] A. Roucoux, J. Schulz, H. Patin, *Chem. Rev.* **2002**, *102*, 3757−3778.
[8] S. Özkar, R. G. Finke, *Mater. Adv.* **2021**, *2*, 186–235.
[9] F. Fiévet, S. Ammar-Merah, R. Brayner, F. Chau, M. Giraud, F. Mammeri, J. Peron, J.-Y. Piquemal, L. Sicarda, G. Viau, *Chem. Soc. Rev.* **2018**, *47*, 5187-5233.
[10] D. Baudouin, K. C. Szeto, P. Laurent, A. De Mallmann, B. Fenet, L. Veyre, U. Rodemerck, C. Copéret, C. Thieuleux, *J. Am. Chem. Soc.* **2012**, *134*, 20624–20627.
[11] T. Galeandro-Diamant, I. Suleimanov, L. Veyre, M. Bousquié, V. Meille, C. Thieuleux, *Catal. Sci. Technol.* **2019**, *9*, 1555–1558.
[12] M. Jakoobi, V. Dardun, L. Veyre, V. Meille, C. Camp, C. Thieuleux, *J. Org. Chem.* **2020**, *85*, 11732–11740.
[13] R. Azuma, S. Nakamichi, J. Kimura, H. Yano, H. Kawasaki, T. Suzuki, R. Kondo, Y. Kanda, K. I. Shimizu, K. Kato, et al., *ChemCatChem* **2018**, *10*, 2378–2382.
[14] T. Ahmad, R. Phul, H. Khan, *Curr. Org. Chem.* **2019**, *23*, 994–1004.
[15] M. Muzzio, J. Li, Z. Yin, I. M. Delahunty, J. Xie, S. Sun, *Nanoscale* **2019**, *11*, 18946–18967.
[16] M. Poliakoff, J. J. Turner, *J. Chem. Soc. A Inorganic, Phys. Theor.* **1971**, 654–658.
[17] N. N. Greenwood, T. C. Gibb, *Mössbauer Spectroscopy*, Chapman And Hall Ltd, London, UK, **1971**.
[18] F. Grandjean, G. J. Long, C. G. Benson, U. Russo, *Inorg. Chem.* **1988**, *27*, 1524–1529.
[19] R. Greatrex, N. N. Greenwood, *Discuss. Faraday Soc.* **1969**, *47*, 126–135.
[20] M. Boualleg, D. Baudouin, J. M. Basset, F. Bayard, J. P. Candy, J. C. Jumas, L. Veyre, C. Thieuleux, *Chem. Commun.* **2010**, *46*, 4722–4724.
[21] O. Mathon, A. Beteva, J. Borrel, D. Bugnazet, S. Gatla, R. Hino, I. Kantor, T. Mairs, M. Munoz, S. Pasternak, et al., *J. Synchrotron Radiat.* **2015**, *22*, 1548–1554.
[22] J. L. Tirado, P. Lavela, C. Pérez Vicente, B. León, C. Vidal-Abarca, *Hyperfine Interact.* **2012**, *207*, 53–59.
[23] A. N. Nesmeyanov, R. K. Freidlina, E. C. Chukovskaya, R. G. Petrova, A. B. Belyavsky, *Tetrahedron* **1962**, *17*, 61–68.
[24] C. C. Hojilla Atienza, A. M. Tondreau, K. J. Weller, K. M. Lewis, R. W. Cruse, S. A. Nye, J. L. Boyer, J. G. P. Delis, P. J. Chirik, *ACS Catal.* **2012**, *2*, 2169–2172.
[25] A. M. Tondreau, C. C. H. Atienza, K. J. Weller, S. A. Nye, K. M. Lewis, J. G. P. Delis, P. J. Chirik, *Science* **2012**, *335*, 567–570.
[26] D. Peng, Y. Zhang, X. Du, L. Zhang, X. Leng, M. D. Walter, Z. Huang, *J. Am. Chem. Soc.* **2013**, *135*, 19154–19166
[27] M. D. Greenhalgh, D. J. Frank, S. P. Thomas, *Adv. Synth. Catal.* **2014**, *356*, 584–590
[28] Y. Sunada, D. Noda, H. Soejima, H. Tsutsumi, H. Nagashima, *Organometallics* **2015**, *34*, 2896–2906
[29] D. Noda, A. Tahara, Y. Sunada, H. Nagashima, *J. Am. Chem. Soc.* **2016**, *138* , 2480–2483.
[30] A. Sanagawa, H. Nagashima, H. *Organometallics* **2018**, *37*, 2859–2871.
[31] B. Basu, R. Gilbert-Wilson, D. L. Gray, T. B. Rauchfuss, A. K. Dash, *Organometallics* **2018**, *37*, 2760–2768.
[32] R. Azuma, S. Nakamichi, J. Kimura, H. Yano, H. Kawasaki, T. Suzuki, R. Kondo, Y Kanda, K. Shimizu, K. Kato, O. Yasushi *ChemCatChem* **2018**, *10* , 2378–2382.
[33] J. Haber, J. H. Block, B. Delmon, *Pure & Appl. Chem.* **1995**, 67, 1257-1306.

Entry for the Table of Contents

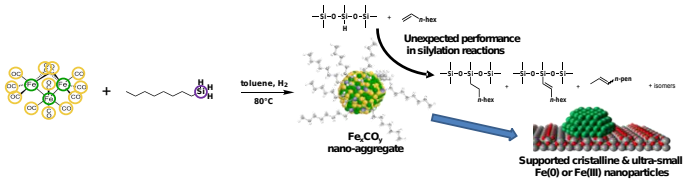

Very small non-crystalline and non-metallic iron-based nanoparticles were prepared in solution using commercially available reagents. While classical crystalline Fe nanoparticles were inactive in alkene hydrosilylation, these Fe_xCO_y nano-aggregates in solution were found active in 1-octene hydrosilylation with 1,1,1,2,3,3,3-heptamethyltrisiloxane (MD'M). From such Fe_xCO_y nano-aggregates in solution, well-defined solids containing either iron and iron oxide NPs were also easily prepared.